Journal of Power Sources 248 (2014) 1007–1013

Contents lists available at ScienceDirect

Journal of Power Sources

journal homepage: www.elsevier.com/locate/jpowsour

Coated stainless steel 441 as interconnect material for solid oxide fuel cells: Oxidation performance and chromium evaporation☆

J.G. Grolig*, J. Froitzheim, J.-E. Svensson

Environmental Inorganic Chemistry, Chalmers University of Technology, Kemivägen 10, SE-41296 Gothenburg, Sweden

HIGHLIGHTS

- We exposed coated AISI 441 in a SOFC cathode side atmosphere.
- The oxidation and chromium volatilization were monitored.
- RE coated 441 showed improved corrosion resistance and no oxide scale spallation.
- RE/Co-coated 441 showed superior corrosion behaviour and low chromium evaporation.

ARTICLE INFO

Article history:
Received 31 May 2013
Received in revised form
9 August 2013
Accepted 18 August 2013
Available online 12 September 2013

Keywords:
Interconnect
Chromium volatilization
AISI 441
Reactive elements
SOFC

ABSTRACT

Reactive Element (RE) and RE/cobalt-coated stainless steel AISI 441 was exposed at Solid Oxide Fuel Cell (SOFC) cathode conditions (850 °C in air with 3% water content) for up to 500 h. The chromium evaporation was measured by applying the denuder technique. Uncoated material exhibited severe spallation which could be successfully prevented by using cerium or lanthanum coatings. By applying double layer coatings of cerium or lanthanum in combination with cobalt the oxidation rate was decreased and the chromium volatilisation was also about 90% lower than the uncoated material.

1. Introduction

Solid Oxide Fuel Cell (SOFC) technology is considered to be promising in the fields of decentralised electricity and heat production. To achieve high voltage output, planar fuel cell elements so-called PEN elements (positive electrode, electrolyte, negative electrode) consisting of an anode, an electrolyte and a cathode which are stacked together [1]. So called interconnectors are needed to stack these PEN elements. The functions of interconnects are not only the electrical connection between two PEN elements but also the separation of the anode atmosphere of one cell from the cathode atmosphere of the following cell. The requirements for interconnects, among others, are an expansion coefficient similar to the ceramic components of the PEN element, high temperature stability, high electrical conductivity, good gas tightness and low production costs.

Recent developments, such as a thinner electrolyte thickness and improved cathodes, have resulted in lower operating temperatures of about 600–800 °C [2,3]. An advantage of these lower operation temperatures is the larger choices of potential interconnect materials. At high temperatures mainly ceramic materials have been applied, whereas at lower temperatures ferritic steels can also be used for an interconnect application. The advantages of these steels are a similar expansion coefficient, good durability, relatively high electronic conductivity, mechanical durability and they are also more economical. Most promising for an interconnect

* Corresponding author. Tel.: +46 772 2828; fax: +46 772 2853.
E-mail address: jan.grolig@chalmers.se (J.G. Grolig).

0378-7753
http://dx.doi.org/10.1016/j.jpowsour.2013.08.089

application are ferritic steels with a chromium content between 18 and 25%.

These steels form a protective chromia layer when exposed to an SOFC cathode atmosphere. However, the protective chromia scale of the steel leads to degradation of the fuel cell due to the volatilization of $CrO_2(OH)_2$, which reacts at the cathode/electrolyte/atmosphere triple points, leading to so called cathode poisoning [4,5]. Early studies on conventional commercial ferritic stainless steels have shown that they lack sufficient corrosion resistance for most interconnect applications. This leads to the development of tailor-made steels not only to increase creep strength and corrosion resistance but also to decrease chromium evaporation. Some examples of these steels are Crofer 22 APU and Crofer 22 H from ThyssenKrupp VDM, Sandvik Sanergy HT from Sandvik Materials Technology AB or ZMG 232 G10 from Hitachi Metals [6,7]. All of the steels have additions of about 0.5 wt.% manganese, leading to the formation of an outer chromium manganese spinel layer during exposure. This phase reduces chromium evaporation by about 60–70% [8].

In order to improve corrosion resistance, the above-mentioned steels contain so called Reactive Elements (RE), e.g. cerium, lanthanum, yttrium, neodymium or zirconium. The beneficial effect of REs has been discussed for several decades and different mechanisms have been proposed, which is beyond the focus of this paper [9–11]. Besides small additions of REs to the steel it has been shown that RE coatings can also have a beneficial effect on the corrosion performance of the steel in SOFC relevant atmospheres [12–14].

Chromium evaporation can be decreased by thin film coatings, which can be classified into two main groups; first perovskite structure and second spinel structure coatings.

Up to now various perovskite coatings for corrosion protection and the prevention of chromium evaporation have been applied; Stanislowski et al. have applied various lanthanum-based ceramics such as LSC ($LaScCrO_3$) or LSM ($LaSrMnO_3$) in thicknesses between 32 and 45 μm [8]. The coated samples exhibited lower chromium evaporation, but some of the coatings suffered spallation. Kurokawa et al. have also studied LSM ($LaSrMnO_3$) and LSCF ($LaSrCoFeO_3$) and found a significant decrease in chromium evaporation [15]. A common drawback of perovskite coatings are often difficulties in the adhesion of the coatings [16].

Spinel coatings are the second class of coatings commonly proposed. The ones most referred to in the literature are coatings based on cobalt and its oxides combined with other transition metals. Different thin film technologies have also been employed to apply spinel coatings. Stanislowski et al. have tested cobalt, nickel and copper coatings, which were applied via sputter coating on Crofer 22 APU, and found that all coatings decreased chromium evaporation significantly. Yang et al. have investigated $Mn_{1.5}Co_{1.5}O_4$ spinel coatings, prepared with a slurry-coating process, on AISI 441, and found that these coatings increased corrosion resistance and decreased electrical resistance [17].

Besides these coatings for the prevention of chromium evaporation, combinations of RE coatings with spinel structure coatings have been developed and investigated. Qu et al. have combined yttrium with cobalt coatings prepared via a sol–gel route and have investigated their corrosion and electronic properties. They found that the combined coating had lower resistances than single-coated samples [18]. Froitzheim et al. have shown a beneficial effect by combining cerium coatings with cobalt coating, where both the oxidation and the chromium evaporation could be lowered significantly [19].

The above cited studies exemplify that uncoated ferritic stainless steels are not suitable for almost all SOFC applications. Therefore, if coating steel is inevitable, the combination of a low cost steel substrate with a coating that provides the required surface properties seems worthwhile investigating; particularly since the interconnect can, according to Hall et al. [20] comprise up to 45% of the total stack costs.

Type 441 stainless steel is, from an economic point of view, very promising but its corrosion performance in SOFC environments is not sufficient for a long-term operation [6]. This is mainly attributed to the higher silicon content and lower silicon to niobium ratio [6] and the lack of reactive elements. The aim of this investigation, therefore, is to determine if the corrosion resistance of type 441 stainless steel can be enhanced by applying so-called reactive element coatings, and if combinations of reactive element coatings and cobalt coatings can enhance the chromium evaporation performance of this stainless steel and additionally show an improvement in corrosion performance.

2. Experimental

2.1. Sample preparation

Pre-coated and uncoated steel strips of AISI 441 (compositions given in Table 1) received in sheets of 0.2 mm thickness from Sandvik Materials Technology AB were cut to coupons of 15 × 15 mm. The coatings were applied by physical vapour deposition and coating thickness was measured during the deposition process via a quartz crystal balance. Metallic targets were used; although in the case of the Ce and La coatings it might be expected that these form oxides during the deposition process. The samples were ultrasonically cleaned first in acetone and afterwards in ethanol for 20 min for each step. After cleaning, the samples were dried and weighted on a Sartorius MC5 scale.

2.2. Exposure

The samples were exposed using the denuder technique; described in more detail elsewhere [21]. The experiments were performed in a tubular furnace equipped with a flow restrictor of silicon carbide to ensure turbulent flow. A so-called denuder tube was placed at the outlet of the furnace, coated with sodium carbonate to collect evaporated chromic species. The reaction between the evaporated chromium-oxy-hydroxy species and sodium carbonate is shown in equation (1).

$$CrO_2(OH)_2 + Na_2CO_3 \rightarrow Na_2CrO_4 + H_2O + CO_2 \quad (1)$$

The denuder tubes were changed regularly and washed out with MQ water, the chromium concentration of the solution was measured using photo spectroscopy. By knowing the samples' geometry and by calibrating the photo spectrometer for chromium concentration it is possible to relate the amount of evaporated chromium to the exposed sample area.

Table 2 lists the different tested samples. To quantify chromium evaporation, the samples were exposed isothermally to a temperature of 850 °C for 500 h in air, which contained 3% water vapour. The tested environment was chosen to simulate a relatively harsh, due to high humidity and temperature cathode side environment. Since the focus of this study was concerning cathode side corrosion and the effect of chromium evaporation the samples were only exposed to a cathode side environment, which is in contrast to real

Table 1
Batch-specific values provided by the manufacturer, given in wt. %.

	Fe	Cr	C	Mn	Si	S	P	Ni	Nb	Ti
Wt. %	Bal.	17.83	0.012	0.26	0.55	0.002	0.024	0.13	0.48	0.14

Table 2
Investigated coating systems.

Sample name	Inner coating	Outer coating
Uncoated	–	–
Ce coated	10 nm cerium	–
La coated	10 nm lanthanum	–
Ce/Co coated	10 nm cerium	620 nm cobalt
La/Co coated	10 nm lanthanum	620 nm cobalt

SOFC conditions. The flow rate was set to a value of 6000 mL min^{-1} which has been shown in previous studies to be in the flow-independent regime of chromium evaporation and can be transferred to a flow of approx. 27 cm s^{-1} [21]. Corrosion performance was additionally tested by exposing different samples discontinuously at intervals of increasing duration at the same temperature and flow for a total time of 570 h. After each interval, the samples were cooled to room temperature and weighted before reheating.

3. Results

3.1. Gravimetric measurements

The samples were exposed discontinuously at 850 C. Fig. 1 shows the mass gain of the different samples. After 570 h of exposure, the uncoated substrate material had a mass gain of 0.48 mg cm^{-2}. After about 100 h of exposure, the uncoated material started to suffer from spallation. The cerium-coated material exhibited a mass gain of about 0.45 mg cm^{-2} and lanthanum coated material of about 0.52 mg cm^{-2} after a total exposure time of 570 h. After an exposure time of 570 h the cerium/cobalt material had a mass gain of 0.59 mg cm^{-2} and the lanthanum/cobalt coated material 0.58 mg cm^{-2}. Both of the RE/cobalt-coated samples had a mass gain of about 0.21 mg cm^{-2} after only 100 min of exposure. After an exposure time of 100 min all coated samples exhibited parabolic corrosion behaviour. The mass gain of the coated samples exposed discontinuously did not differ significantly from isothermal exposed samples. It was observed that the lanthanum/cobalt samples were slightly bent after exposure.

3.2. Chromium evaporation

The chromium evaporation was conducted in a separate series of experiments and samples were exposed isothermally. Fig. 2 shows

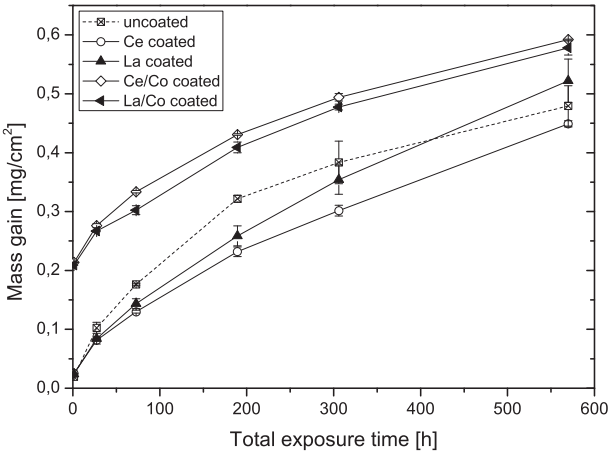

Fig. 1. Mass gain of different coated AISI 441 specimens during discontinuous exposure at 850 °C.

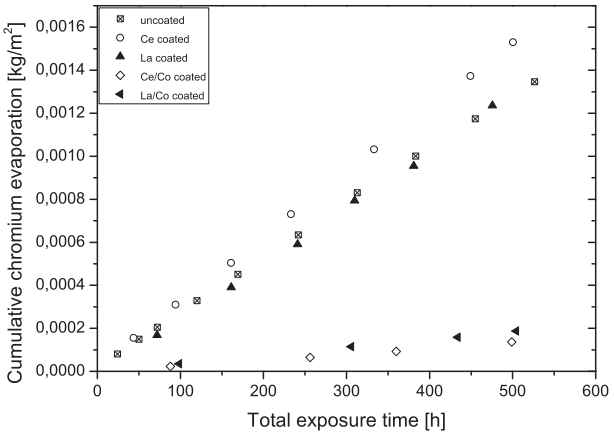

Fig. 2. Cumulative chromium evaporation of different coated AISI 441 specimens during isothermal exposure at 850 °C.

the cumulative chromium evaporation of five different material combinations. The uncoated material as well as the lanthanum coated material exhibited similar chromium evaporation. The uncoated material evaporated a total mass of about 0.0014 kg m^{-2} chromium after 526 h of exposure. The lanthanum-coated material evaporated 0.0012 kg m^{-2} chromium after 475 h of exposure time. The cerium-coated material evaporated 0.0015 kg m^{-2} chromium after 500 h, which is about 10% higher compared to the uncoated and lanthanum-coated materials. The cerium/cobalt-coated material showed a drastic reduction in chromium evaporation of about 0.00014 kg m^{-2} and lanthanum/cobalt-coated material showed a reduction of about 0.00019 kg m^{-2} after about 500 h of exposure time.

3.3. Microstructural investigation

The surface of the uncoated material appeared to be buckled with a linear texture (see Fig. 3a). The oxide scale was spalled off at various positions and this observation was consistent for all uncoated samples with exposure times longer than 100 h. The cross-sectional micrograph showed a double-layered oxide with a very thin (~0.8 μm) outer oxide layer and a thick (~3.6 μm) inner oxide layer (see Fig. 3b). An EDX analysis revealed that the outer oxide layer contained relatively high amounts of manganese, whereas the inner layer contained relatively pure chromium oxide. A zone of internal titanium oxides was clearly visible beneath the oxide scale. Several Laves phase precipitates, rich in silicon and niobium, were also observed. The locations were predominantly along grain boundaries. The zone of internal oxidation as well as the Laves phases was consistent for all samples.

The cerium-coated sample exhibited a buckled surface with a linear texture (see Fig. 4a). In contrast to the uncoated samples, the cerium-coated samples showed no spallation. The cross-section of the cerium-coated sample confirmed the buckled oxide scale and a double-layered oxide similar to the uncoated substrate (see Fig. 4b). The thickness of the inner oxide layer was approximately 2.3 μm, and the outer layer was about 0.5 μm thick.

The surface of the lanthanum-coated sample appeared to have a structure similar to the uncoated and the cerium-coated sample (see Fig. 5a), but the linear texture was slightly more distinct. No spallation was observed for the lanthanum-coated samples. A cross-sectional micrograph shown in Fig. 5b shows, as in the previous cases, a double-layer oxide with an inner oxide layer thickness of 2.1 μm and an outer oxide layer thickness of 0.8 μm. A comparison of EDX line scans between the uncoated and the RE-

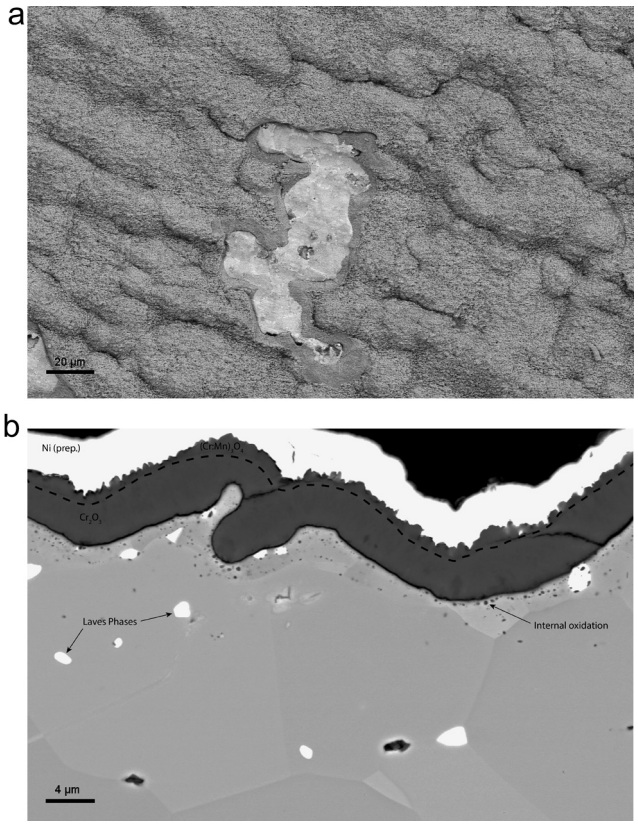

Fig. 3. a–b. BSE micrographs of uncoated AISI 441 exposed for 500 h at 850 °C (top view a, cross-section b).

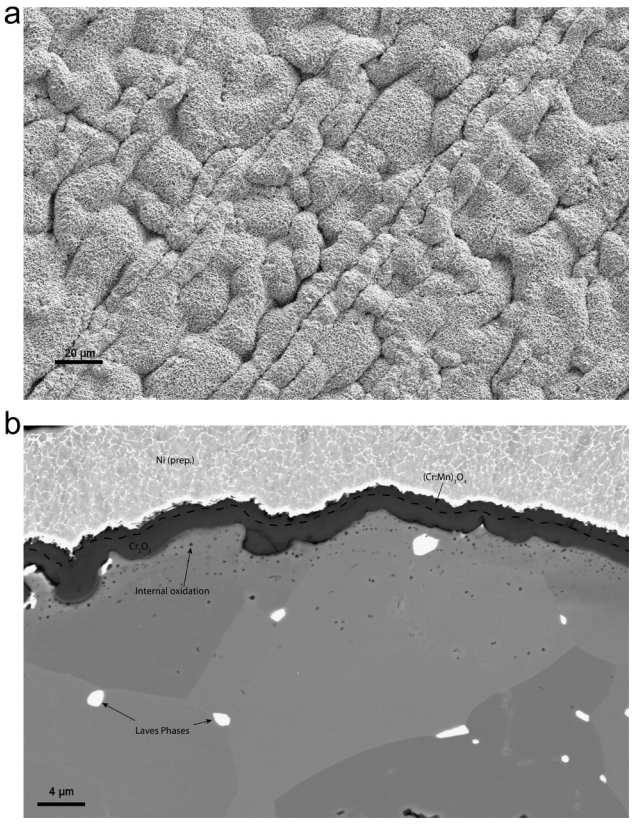

Fig. 5. a–b. SEM micrographs of lanthanum-coated AISI 441 exposed for 500 h at 850 °C (top view a (SE), cross-section b (BSE).

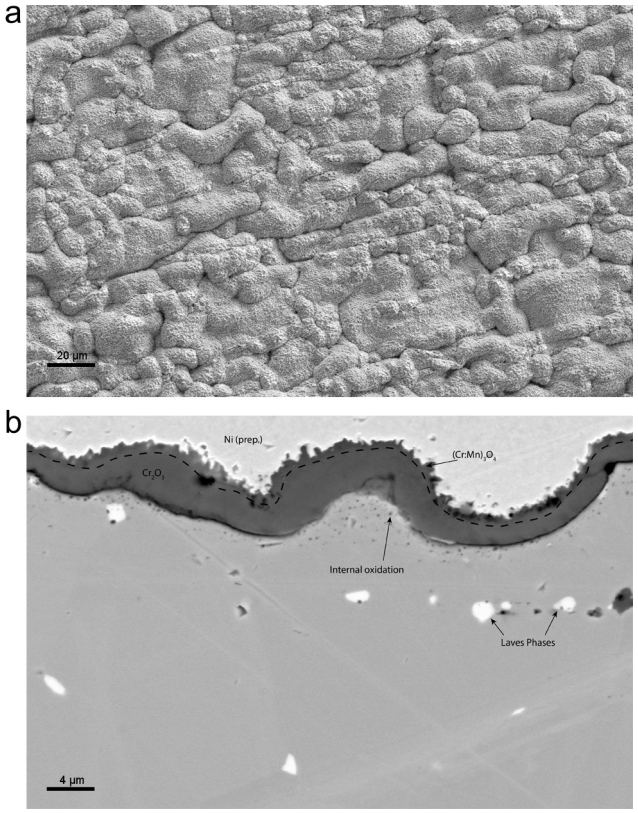

Fig. 4. a–b. SEM micrographs of cerium-coated AISI 441 exposed for 500 h at 850 °C (top view a (SE), cross-section b (BSE)).

coated samples showed no significant differences, so for the sake of simplicity only the lanthanum-coated sample line scan is shown here (see Fig. 6).

The surface of the cerium/cobalt-coated samples appeared to be less wavy than the uncoated and RE-coated samples, even though the linear texture observed on the uncoated and RE-coated samples could still be seen (see Fig. 7a). The cross-section in Fig. 7b confirms the decrease in waviness. Furthermore, the oxide scale consisted of a double layer; an outer layer that was cobalt and manganese rich and about 1.9 µm thick, and an inner layer that was, similar to the

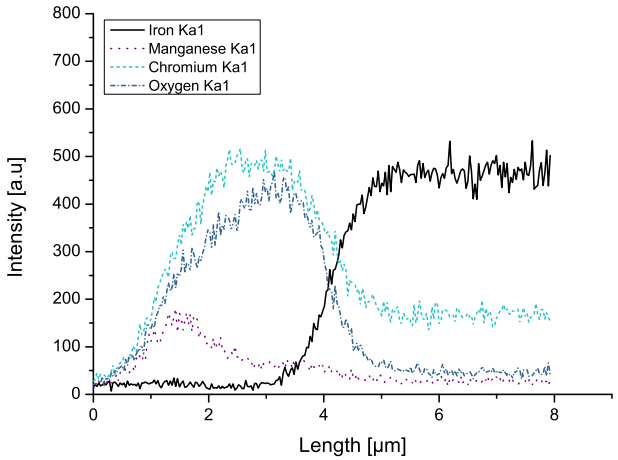

Fig. 6. EDX line scan of La-coated AISI 441 exposed for 500 h at 850 °C (Si and La below detection limit).

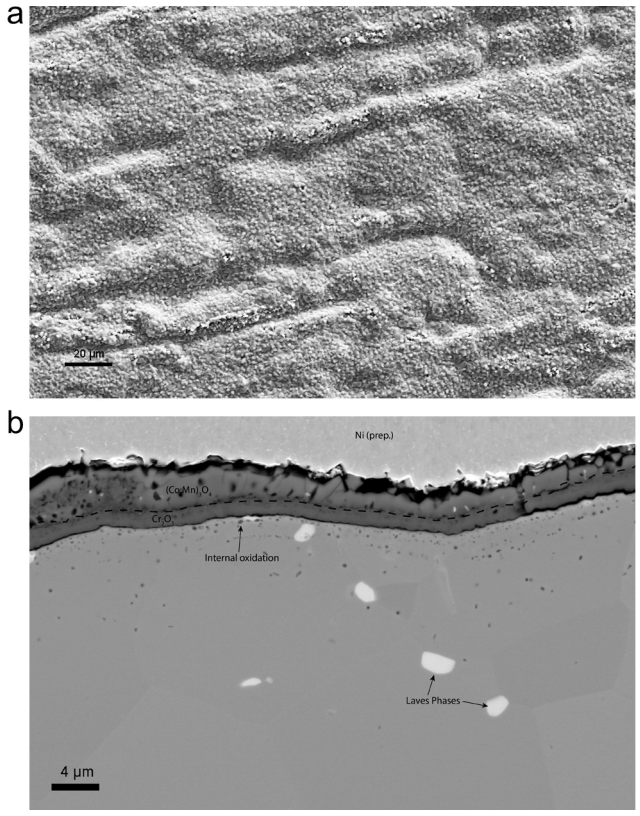

Fig. 7. a–b. SEM micrographs of cerium/cobalt-coated AISI 441 exposed for 500 h at 850 °C (top view a (SE), cross-section b (BSE)).

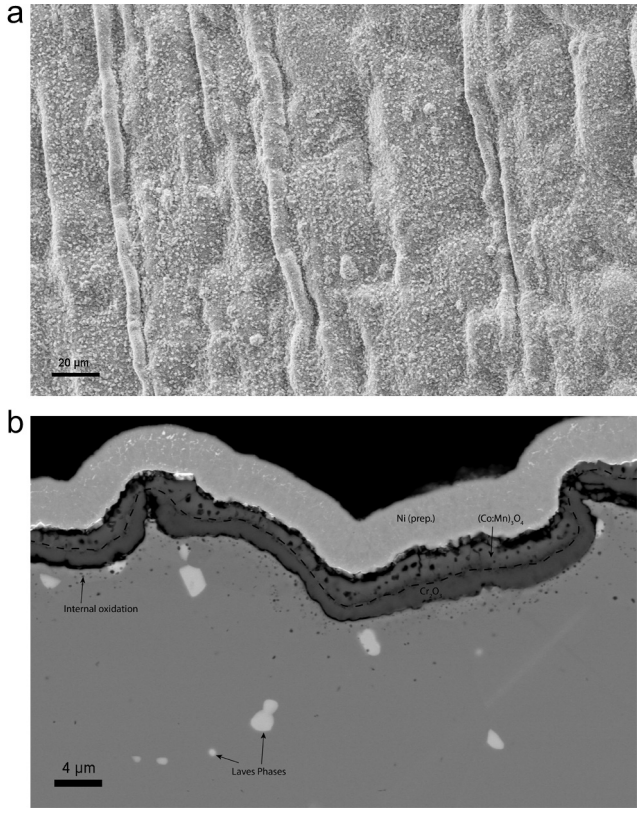

Fig. 8. a–b. SEM micrographs of lanthanum/cobalt-coated AISI 441 exposed for 500 h at 850 °C (top view a (SE), cross-section b (BSE)).

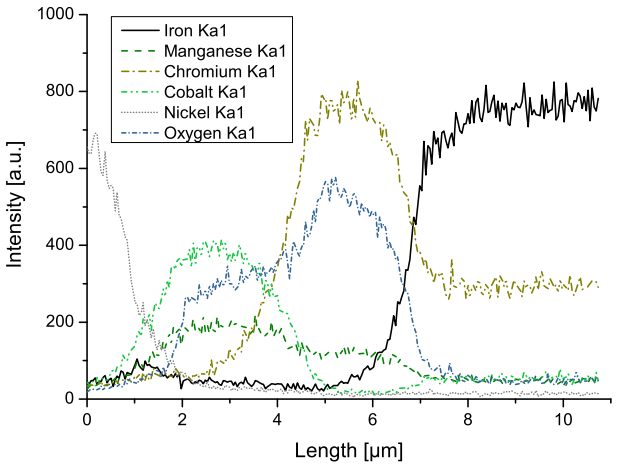

Fig. 9. EDX line scan of La/Co-coated AISI 441 exposed for 500 h at 850 °C (Si and La below detection limit).

previous cases, chromium rich and approximately 1.4 µm thick. Some small pores were observed between the two oxide layers.

Fig. 8a shows the surface of a lanthanum/cobalt-coated sample. Several linear wrinkles were observed. The cross-section (see Fig. 8b) revealed that, similar to the cerium/cobalt-coated sample, a large number of pores were present in the oxide scale of the lanthanum/cobalt-coated sample. In contrast to the cerium/cobalt-coated samples, pores in the outer layer, and not only at the oxide–oxide interface, were detected (see Fig. 8b). The EDX line scan of the oxide scale of the lanthanum/cobalt-coated was similar to the cerium/cobalt-coated samples and is therefore the only one shown here (see Fig. 9). For a better comparison Table 3 provides the approximate oxide thicknesses.

4. Discussion

4.1. Resistance against oxidation

Oxidation resistance is the major lifetime limiting factor for metallic interconnects. Lifetime prediction is usually based on mass gain, but in the present case there are two complications that affect mass gain measurements, the chromium evaporation that causes a continuous mass loss and the almost immediate oxidation of the metallic cobalt coating. Froitzheim et al. have shown that the process of cobalt oxidation takes approximately 30 s for this type of coating [22]. The data obtained from mass gain and chromium evaporation were used to calculate the oxidation properties. The almost immediate oxidation of the cobalt top coating was subtracted from the mass gain (for the cobalt coated samples) by assuming a weight gain of 0.202 mg cm^{-2} for the oxidation of a 630 nm cobalt coating to Co_3O_4. In a second step the evaporated chromium was added to the mass gain by assuming the evaporation

Table 3
Compilation of approximate oxide layer thicknesses.

Material	Inner oxide layer thickness [µm]	Outer oxide layer thickness [µm]	Total oxide thickness [µm]
Uncoated	3.5 ± 0.2	0.8 ± 0.1	4.3
Ce coated	2.3 ± 0.4	0.5 ± 0.1	2.8
La coated	2.1 ± 0.5	0.8 ± 0.1	2.9
Ce/Co coated	1.4 ± 0.1	1.9 ± 0.4	3.2
La/Co coated	1.6 ± 0.2	1.6 ± 0.3	3.2

of Cr_2O_3 and a constant evaporation rate. Every mg of lost chromium is equal to 1.46 mg of Cr_2O_3 oxide scale. The resulting graph is shown in Fig. 10 and should give a better understanding of the influence of the various coatings on the oxidation rate. The data presented in Fig. 1 have been obtained in a discontinuous exposure and Cr evaporation measurement was carried out isothermally. Although thermal cycles are known to affect the oxidation behaviour this effect is expected to be of minor importance in the present case due to the limited number of thermal cycles and because the mass gain data between both exposures do not differ significantly. Since the uncoated substrate material suffered severe spallation it is not included in the graph.

The lanthanum-coated samples, represented by the filled upwards pointing triangles had the highest oxidation rate; whereas the cerium-coated samples (hollow circles) oxidized slower.

The most explicit effect in this graph is the influence of the cobalt top coating on oxidation resistance. Both the cerium/cobalt-coated (hollow diamonds) and the lanthanum/cobalt-coated (filled left pointing triangles) samples oxidized at a similar rate and the outer cobalt coating decreased the oxidation significantly. This observation was not seen by applying similar coatings to Fe–22Cr interconnect steels such as Sandvik Sanergy HT [22]. In a different study by Yang et al. $Mn_{1.5}Co_{1.5}O_4$ coatings on AISI 441 reduced the oxidation rate drastically as the authors proposed an effect of limited oxygen inward diffusion. In contrast to the present investigation their coating thickness was not given but appeared to be in the range of several micrometres [17].

4.2. Chromium evaporation

The chromium evaporation shown in Fig. 2 followed a relatively linear trend for all materials, even if the initial evaporation was slightly higher. For the uncoated, cerium- and lanthanum-coated samples one can assume a growing chromium manganese spinel as an outer oxide layer. This layer is in the initial stages very thin and therefore not yet totally effective in retaining chromium.

The effect of cerium on chromium evaporation is interesting for the reactive element coatings; the slightly higher evaporation of the cerium-coated samples compared to the lanthanum-coated samples could either be a catalytic effect of cerium on the process of chromium evaporation or a result of a slower outward diffusion of manganese ions. A slower diffusion of manganese outward would lead to a thinner outer chromium manganese spinel. The effect of a thinner outer spinel cannot be proven by the investigated exposure times, even though one might see a trend of a slightly thinner outer spinel for the cerium coated samples in the SEM micrographs (Figs. 4b and 5b). The argument for a slower manganese outward diffusion could also be supported by the lower oxidation rate, which might also be caused by a slower diffusion of manganese outward.

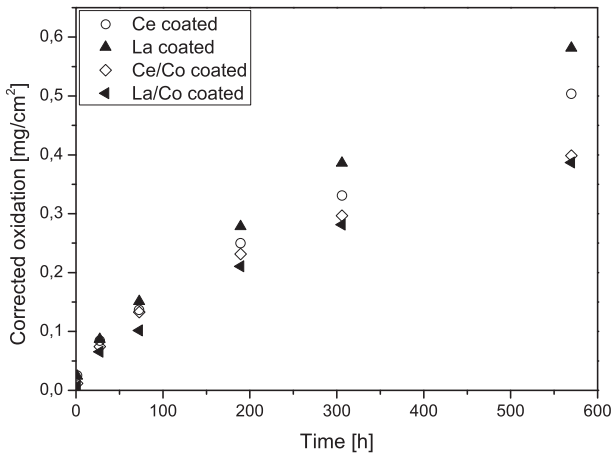

Fig. 10. Corrected oxidation of the different coated AISI 441. The mass gain due to the initial oxidation of the Co layer is subtracted and the mass loss due to Cr evaporation is added.

The chromium evaporation was almost linear for the cerium/cobalt- and lanthanum/cobalt-coated samples. Since almost immediately after heating up to exposure temperature the cobalt layer oxidises to Co_3O_4 [22] the chromium retention is already given. After time manganese diffuses outwards and a cobalt manganese spinel is formed. This spinel seems to be even more effective than the cobalt oxide in decreasing chromium evaporation, which could be an effect of a simply thicker outer oxide layer, or it could be due to a lower diffusion coefficient of chromium ions in the manganese-doped spinel layer.

4.3. Oxide scale evolution

The amount of spallation on the uncoated material observed in this study is high compared to other studies. Liu et al. observed spallation on AISI 441 during experiments in stagnant air, unfortunately the chemical composition of the investigated steel is not given [23]. In line with the observation of this study are Yang et al.; they reported spallation to a lower extent and at longer exposure times, which one might suspect is due to a lower exposure temperature (800 °C) [17]. Since the silicon content in the investigated batch was comparably high (0.55 wt.%) and the exposure temperature at the upper limit of a SOFC application, it was expected that the amount of Laves phase formation was not sufficient to tie up all the silicon contained in the steel and prevent subscale silica formation, which is commonly suggested to cause spallation [6]. This is supported by the observations of Jablonski et al., who concluded that the niobium content as well as the too high exposure temperature do not allow for the complete capture of all silicon since the concentration of the Laves phase decreases with increasing temperature [6]. In addition, the silicon content in Jablonski's investigation was, with about 0.33 wt. %, much lower than in this study.

Both reactive element coatings improved the adhesion of the oxide scales significantly which is in line with the observations from other studies [24,25]. Even though the exposure temperatures are relatively low for applying reactive element coatings, the observed improved adhesion is in line with the findings of Belogolovsky et al. [25] who have shown improved scale adhesion for yttrium-nitrate-coated stainless steel 430. Different mechanisms have been proposed to explain this observation; such as a reduction in growth rate, enhanced scale plasticity, a reduction in growth stress or a strengthened scale alloy interface [9,26].

As mentioned above the formation of a silica layer at the metal/oxide interface is often considered as the most relevant mechanism for oxide spallation on this type of material. Although the batch of type 441 investigated in the present study had a relatively high Si content no significant subscale silica formation was observed. In order to corroborate this finding two focused ion beam (FIB) prepared cross-sections of an uncoated and a cerium-coated sample were EDX analyzed. The line scans are presented in Fig. 11. Minor subscale silica enrichment was found in both cases. Consequently it must be concluded that not all Si was tied up by the Laves phase precipitates but that small amounts of Si segregated at the metal/oxide interface. However, the fact that only the uncoated samples exhibited spallation while Si segregation was observed in both cases indicates that Si was

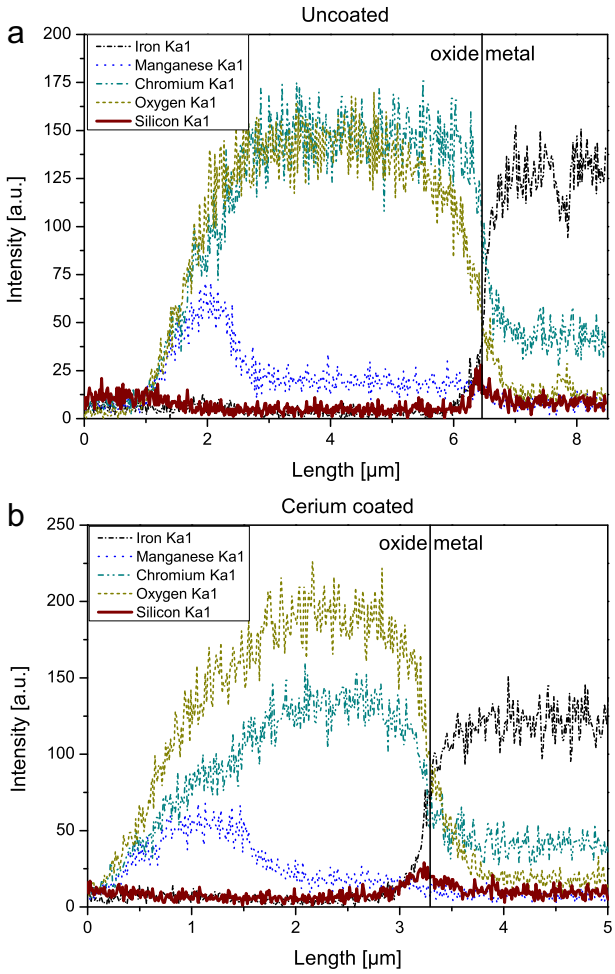

Fig. 11. a–b. EDX line scans of FIB prepared uncoated (a) and cerium-coated (b) after 500 h at 850 °C of exposure.

not the detrimental factor for scale adhesion in the present study. The improved adhesion of the oxide scale in the presence of REs is a well-known effect although the effectiveness of RE-coatings has to be proven for longer exposure times [9,10,27].

Depicted in the SEM micrographs (Figs. 3–5 and 7–8) all samples exhibited a wavy linear textured surface. This was more pronounced for the uncoated and RE-coated samples whereas the RE/cobalt-coated samples, especially the cerium/cobalt-coated samples, had a smoother surface.

It is well known that surface treatment can lead to differences in oxidation behaviour [24,25,28]. The linear texture is parallel to the rolling direction as it was proven in a separate experiment. Therefore one might suspect that the surface roughness induced by the rolling process lead to the observed wavy surfaces. For the cerium/cobalt and lanthanum/cobalt samples the effect is less clear, which could be due to the smoothening effect of the cobalt coating prior to exposure. An explanation for the smoothening effect can be the volume expansion in the initial stages of oxidation when the cobalt top coating is transformed to cobalt oxide.

Further experiments or stack tests should be conducted; further lab tests should include longer exposure times and preferably also lower temperatures to ensure stability also for a long term application. Since this investigation was dedicated to a cathode atmosphere, further investigations in an anode or a dual atmosphere should be performed.

5. Conclusion

This investigation shows strong potential for AISI 441 as an SOFC interconnect material if additional coatings are applied.

Applied coatings of cerium and lanthanum successfully prevented spallation and slowed down the outward diffusion of metal ions and therefore lowered the oxidation rate.

The addition of a cobalt cap layer decreased the oxidation rate even further and reduced chromium evaporation about 90%.

Acknowledgements

Sandvik Materials Technology is acknowledged for providing the samples. The financial support received from The Swedish Research Council and the Swedish Energy Agency (Grant Agreement No 34140-1), The Swedish High Temperature Corrosion Centre as well as the Nordic NaCoSOFC project is gratefully acknowledged. Furthermore, the funding received from the European Union's Seventh Framework Programme (FP7/2007–2013) for the Fuel Cells and Hydrogen Joint Technology Initiative under grant agreement no. [278257] is gratefully acknowledged. Dr. M. Sattari is acknowledged for preparing the FIB cross-sections.

References

[1] A. Evans, A. Bieberie-Hutter, H. Galinski, J.L.M. Rupp, T. Ryll, B. Scherrer, R. Tolke, L.J. Gauckler, Mon. Chem. 140 (2009) 975–983.
[2] I. Kosacki, C.M. Rouleau, P.F. Becher, J. Bentley, D.H. Lowndes, Solid State Ionics 176 (2005) 1319–1326.
[3] F. Mauvy, J.M. Bassat, E. Boehm, J.P. Manaud, P. Dordor, J.C. Grenier, Solid State Ionics 158 (2003) 17–28.
[4] J.W. Fergus, Int. J. Hydrogen Energy 32 (2007) 3664–3671.
[5] W.J. Quadakkers, J. Piron-Abellan, V. Shemet, L. Singheiser, Mater. High Temp. 20 (2003) 115–127.
[6] P.D. Jablonski, C.J. Cowen, J.S. Sears, J. Power Sources 195 (2010) 813–820.
[7] M. Stanislowski, E. Wessel, K. Hilpert, T. Markus, L. Singheiser, J. Electrochem. Soc. 154 (2007) A295–A306.
[8] M. Stanislowski, J. Froitzheim, L. Niewolak, W.J. Quadakkers, K. Hilpert, T. Markus, L. Singheiser, J. Power Sources 164 (2007) 578–589.
[9] P.Y. Hou, J. Stringer, Mater. Sci. Eng. A-Struct. Mater. Prop. Microstruct. Process. 202 (1995) 1–10.
[10] D.P. Whittle, J. Stringer, Philos. Trans. R. Soc. Lond. Ser. A-Math. Phys. Eng. Sci. 295 (1980) 309.
[11] J. Stringer, Mater. Sci. Eng. A-Struct. Mater. Prop. Microstruct. Process. 120 (1989) 129–137.
[12] S. Fontana, R. Amendola, S. Chevalier, P. Piccardo, G. Caboche, M. Viviani, R. Molins, M. Sennour, J. Power Sources 171 (2007) 652–662.
[13] D.E. Alman, P.D. Jablonski, Int. J. Hydrogen Energy 32 (2007) 3743–3753.
[14] S. Canovic, J. Froitzheim, R. Sachitanand, M. Nikumaa, M. Halvarsson, L.G. Johansson, J.E. Svensson, Surf. Coat. Technol. 215 (2013) 62–74.
[15] H. Kurokawa, C.P. Jacobson, L.C. DeJonghe, S.J. Visco, Solid State Ionics 178 (2007) 287–296.
[16] S. Chevalier, C. Valot, G. Bonnet, J.C. Colson, J.P. Larpin, Mater. Sci. Eng. A-Struct. Mater. Prop. Microstruct. Process. 343 (2003) 257–264.
[17] Z.G. Yang, G.G. Xia, C.M. Wang, Z.M. Nie, J. Templeton, J.W. Stevenson, P. Singh, J. Power Sources 183 (2008) 660–667.
[18] W. Qu, L. Jian, D.G. Ivey, J.M. Hill, J. Power Sources 157 (2006) 335–350.
[19] J. Froitzheim, J.E. Svensson, in: S.C. Singhal, K. Eguchi (Eds.), Solid Oxide Fuel Cells 12, Electrochemical Society Inc., Pennington, 2011, pp. 2503–2508.
[20] T.D. Hall, H.A. McCrabb, J. Wu, H. Zhang, X. Liu, E.J. Taylor, in: S.C. Singhal, K. Eguchi (Eds.), Solid Oxide Fuel Cells 12, Electrochemical Society Inc., Pennington, 2011, pp. 2489–2502.
[21] J. Froitzheim, H. Ravash, E. Larsson, L.G. Johansson, J.E. Svensson, J. Electrochem. Soc. 157 (2010) B1295–B1300.
[22] J. Froitzheim, S. Canovic, M. Nikumaa, R. Sachitanand, L.G. Johansson, J.E. Svensson, J. Power Sources 220 (2012) 217–227.
[23] W.N. Liu, X. Sun, E. Stephens, M. Khaleel, Metall. Mater. Trans. A-Phys. Metall. Mater. Sci. 42A (2011) 1222–1228.
[24] N. Shaigan, W. Qu, D.G. Ivey, W.X. Chen, J. Power Sources 195 (2010) 1529–1542.
[25] I. Belogolovsky, P.Y. Hou, C.P. Jacobson, S.J. Visco, J. Power Sources 182 (2008) 259–264.
[26] M. Casteel, D. Lewis, P. Willson, M. Alinger, Int. J. Hydrogen Energy 37 (2012) 6818–6829.
[27] B.A. Pint, in: P.F. Tortorelli, I.G. Wright, P.Y. Hou (Eds.), Proc. John Stringer Symposium on High Temperature Corrosion, ASM International, Materials Park, OH, Indianapolis, 2003, pp. 9–19.
[28] L. Cooper, S. Benhaddad, A. Wood, D.G. Ivey, J. Power Sources 184 (2008) 220–228.